crystals

MDPI

Article

Innovative Method for the Mass Preparation of α''-$Fe_{16}N_2$ Powders via Gas Atomization

Marian Grigoras, Mihaela Lostun *, Marieta Porcescu, George Stoian, Gabriel Ababei * and Nicoleta Lupu

National Institute of Research and Development for Technical Physics, 47 Prof. Dimitrie Mangeron Blvd., 700050 Iasi, Romania; mgrigoras@phys-iasi.ro (M.G.); porcescu@phys-iasi.ro (M.P.); gstoian@phys-iasi.ro (G.S.); nicole@phys-iasi.ro (N.L.)

* Correspondence: mlostun@phys-iasi.ro (M.L.); gababei@phys-iasi.ro (G.A.)

Abstract: The iron nitride materials, especially α''-$Fe_{16}N_2$, are considered one of the most promising candidates for future rare-earth-free magnets. However, the mass production of α''-$Fe_{16}N_2$ powders as a raw material for permanent magnets is still challenging. In this work, starting from iron lumps as a raw material, we have managed to prepare the α''-$Fe_{16}N_2$ powders via the gas atomization method, followed by subsequent nitriding in an ammonia–hydrogen gas mixture stream. The particle size was controlled by changing the gas atomization preparation conditions. X-ray diffractograms (XRD) analyses show that the prepared powders are composed of α''-$Fe_{16}N_2$ and α-Fe phases. The α''-$Fe_{16}N_2$ volume ratio increases with decreasing powder size and increasing nitriding time, reaching a maximum of 57% α''-$Fe_{16}N_2$ phase in powders with size below 32 ± 3 µm after 96 h nitridation. The saturation magnetization reaches the value of 237 emu/g and a reasonable coercivity value of 884 Oe. Compared to the saturation magnetization values of α-Fe powders, the α''-$Fe_{16}N_2$ powders prepared through our proposed approach show an increase of up to 10% in saturation and demonstrate the possibility of mass production of α''-$Fe_{16}N_2$ powders as precursors of permanent magnets without rare earths.

Keywords: $Fe_{16}N_2$ powder; nitridation; gas atomization; magnetic properties; X-ray diffraction

Citation: Grigoras, M.; Lostun, M.; Porcescu, M.; Stoian, G.; Ababei, G.; Lupu, N. Innovative Method for the Mass Preparation of α''-$Fe_{16}N_2$ Powders via Gas Atomization. *Crystals* **2023**, *13*, 1578. https://doi.org/10.3390/cryst13111578

Academic Editor: Duncan H. Gregory

Received: 25 October 2023
Revised: 2 November 2023
Accepted: 8 November 2023
Published: 9 November 2023

1. Introduction

Permanent magnets are indispensable components of modern life and technology, and their influence is constantly growing [1,2]. Today, Nd-Fe-B-based magnets are the most widely used type of permanent magnets due to their outstanding magnetic performance. However, the worries about environmental degradation from rare earth mining, cost, and availability issues have led to a global concern to search for alternatives for rare-earth-free permanent magnets. Thus, it is expected that the next generation of permanent magnets will not contain rare earths, will come from abundant resources, and will have low costs. There are several types of alternative material systems to rare-earth magnets, such as $L1_0$-FeNi [3,4], MnBi [5–7], and α''-$Fe_{16}N_2$. Among them, the α''-$Fe_{16}N_2$ compound with giant saturation magnetization contains widely available, inexpensive, and completely non-polluting elements, making it a promising candidate for rare-earth-free magnets. After the first report by Kim and Takahashi on the giant saturation magnetization of about 290 emu/g of the α''-$Fe_{16}N_2$ phase in the evaporated Fe-N thin film, many researchers have made sustained efforts on both the fundamental [8,9] and practical aspects of preparing of the α''-$Fe_{16}N_2$ material. Thus, several attempts have been successfully made to develop magnetic materials containing α''-$Fe_{16}N_2$ phase in the form of thin films [10–13], foils [14,15], rods [16], ribbons [17], nanocones [18], and nanoparticles and powders [19,20], by using different preparation methods. The reported values of saturation magnetizations were widely scattered from 230 to 315 emu/g and appeared to be inconsistent and sometimes contradictory. However, the value of saturation magnetizations is mainly determined

by the amount of α''-$Fe_{16}N_2$ phase relative to the impurity phases such as α-Fe, γ-Fe-N (austenite), or γ-Fe_4N, in the magnetic material [21]. Therefore, obtaining the magnetic material with pure α''-$Fe_{16}N_2$ phase in sufficiently large quantities is a challenge. On the other hand, the preparation of permanent magnets is naturally related to the precursor material, namely powders. Therefore, various attempts have been made to prepare the α''-$Fe_{16}N_2$ powders by mechanical ball milling of pure iron with a solid nitrogen source, ammonium nitrate [20,22,23], and nanopowders via chemical methods [19,24,25], using a two-step route where several kinds of Fe-oxides such as α-Fe_2O_3, γ-Fe_2O_3, and Fe_3O_4 are reduced to α-Fe in hydrogen atmosphere followed by a low-temperature nitriding. However, the mass production of iron nitrides with nanometer-sized Fe sources has critical drawbacks in manufacturing processes as well as economics. For example, iron oxide particles undergo significant coarsening during the reduction process, resulting in a detrimental effect on the final magnetic properties [19], in addition, due to their small size, the α''-$Fe_{16}N_2$ nanoparticles are highly susceptible to oxidation. Oxidation resistance is slightly modified by coating the α''-$Fe_{16}N_2$ nanoparticles with either Al_2O_3 or SiO_2 in a core–shell arrangement [26,27], but the coating can also contribute to the degradation of the magnetic properties of the resulting particles. A step towards mass production of the α''-$Fe_{16}N_2$ powders was made by introducing the mechanical ball milling of Fe powders together with solid NH_4NO_3 powders for time periods of up to 60 h [22]. The value of the saturation magnetization was about 210 emu/g, the coercivity of 854 Oe, and the volume fraction was about 70%. In a most recent work [23] amorphous powders of $Fe_{78}Si_9B_{13}$ and solid powders of NH_4NO_3 were milled for extended periods of up to 80 h. Although the formation of the α''-$Fe_{16}N_2$ phase was observed, the volume fraction was low, resulting in magnetization of very low saturation at 72.5 emu/g and a moderate coercivity of 541 Oe. A typical and affordable method for the mass production of micrometric metal and alloy powders is the gas atomization technique [28–31]. The idea is to transfer the kinetic energy from a high-velocity gas jet expanded through a nozzle, to a jet of liquid metal, resulting in fragmentation and breaking down into metal droplets. The liquid metal droplets subsequently cool and solidify into metal powder. To date, there is still no report on an approach to preparing α''-$Fe_{16}N_2$ powders via the gas atomization method.

In this paper, we report the successful preparation of α''-$Fe_{16}N_2$ powders using the gas atomization method, followed by subsequent nitriding in the ammonia–hydrogen gas mixture stream.

2. Materials and Methods

The preparation of α''-$Fe_{16}N_2$ powders was carried out in three steps. In the first step, Fe ingots of about 20–25 g were prepared via the arc melting technique from commercial iron lumps (Alfa Aesar) with a purity higher than 99.99%. In the second step, the resulting Fe ingots were used to prepare Fe-N powders via the gas atomization method. This step involves the transformation of a jet of liquid Fe into fine droplets using a high-velocity nitrogen gas. In the last step, the Fe-N powders were nitrided in an NH_3 (92 vol%) + H_2 (8 vol%) gas mixture stream at a flow rate of 100 mL/min, at 150 °C for periods between 12 and 96 h. After cooling to room temperature under the same gas mixture stream, the nitrided powders were immediately transferred to a nitrogen-filled glove box without exposure to air to prepare samples for structural, morphological, and magnetic measurements. The structural analysis was carried out via X-ray diffraction (XRD) in a Bruker AXS D8-Advance diffractometer (Mannheim, Germany) over the angular range 20–90°, with a step of 0.02° and a counting time of 2 s per step, using conventional Cu-Kα incident radiation. The Rietveld refinements of the XRD patterns were performed using the MAUD software package. The microstructure of the sample was investigated using a Scanning Electron Microscope, FIB/FE-SEM Cross-Beam Carl Zeiss NEON 40 EsB (Oberkochen, Germany), equipped with an energy dispersive X-ray spectroscopy (EDS) module. Magnetic measurements were performed using a vibrating sample magnetometer (VSM) (Lake Shore VSM 7410, Westerville, OH, USA) in a maximum applied field of 20 kOe, at room

temperature. The design and operation of the gas atomization facility is described in detail in our previous work [32]. However, for an easy understanding of the atomization process with the homemade equipment used for the preparation of powders, we will reproduce here the gas atomization sketch (Figure 1) as well as some particular characteristics of the configuration we used in the present work. Thus, we mention that the iron ingot was heated and melted via induction in a quartz crucible, and the temperature of the melt before ejection was 1588 °C; both for melt ejection and atomization, respectively, nitrogen gas was used at the ejection pressure of 1 bar and the atomization pressure of 20 bar; the width of the atomizing gas outlet nozzle, which is in the form of an annular slot concentric with the melt jet, was 300 μm; the angle formed between the direction of the melt jet and that of the atomization gas jet was 45°; and the distance between the melt ejection nozzle and the particle collector was 120 cm. In order to prepare powders with different mean particle diameters, the ejection nozzle diameter varied between 100 and 200 μm. Before the melt ejection, the atomization and melting chambers were pressurized for 5 min with nitrogen gas at exposure pressures between 0.5 and 3 bar, to expose the liquid iron to the nitrogen gas.

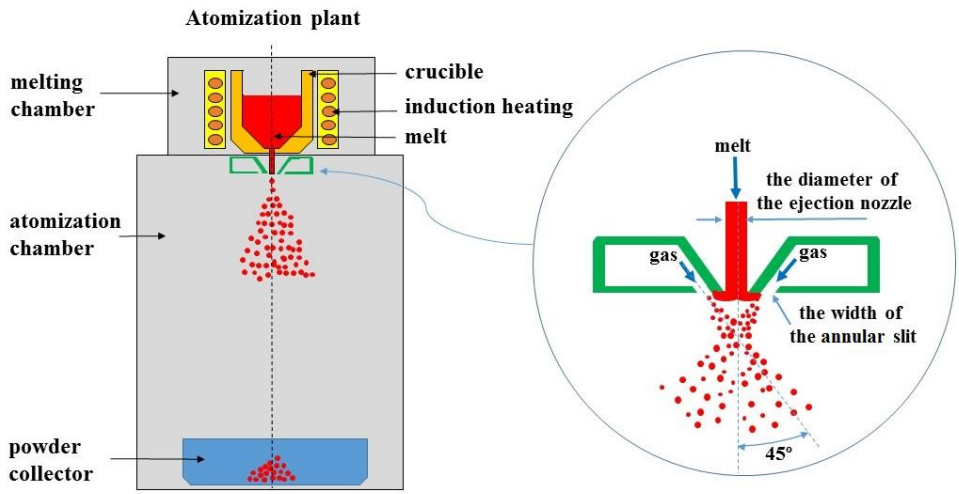

Figure 1. The sketch of the gas atomization plant (**left**) and illustration of the atomization process (**right**). Figure reprinted from [32] under the Creative Commons Attribution (CC BY) license.

3. Results and Discussions

The scanning electron microscope (SEM) images shown in Figure 2 give a short qualitative overview of the powders obtained for different diameters of the ejection nozzles and an exposure pressure of 0.5 bar.

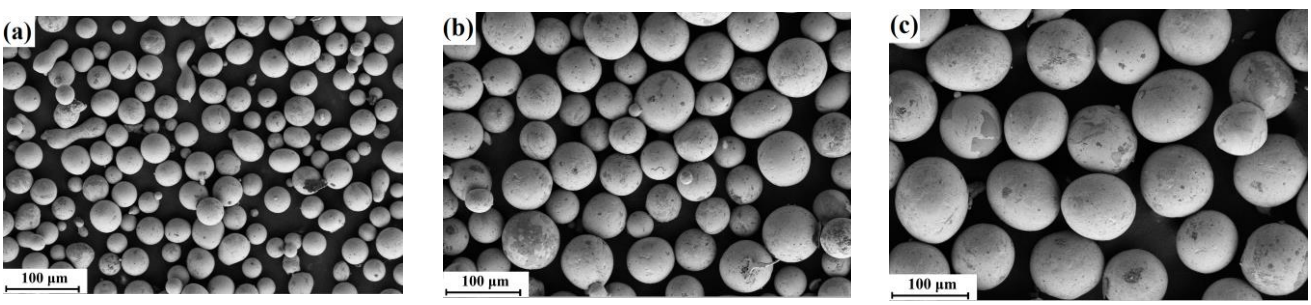

Figure 2. SEM images of Fe-N powders prepared using the melting nozzle with diameters of (**a**) 100 μm, (**b**) 150 μm, and (**c**) 200 μm.

For all the powders, the general particle shape is spherical, and their median diameter increases with the diameter of the ejection nozzle. Thus, the median diameter of the obtained powders is 32 ± 3 μm when an ejection nozzle with a diameter of 100 μm was

used, 58 ± 2 µm for 150 µm, and 96 ± 2 µm for 200 µm. It can be observed that all the powders show a certain amount of satellites, and the finest ones show even particles that have not finished formation. This might be due to the higher cooling rate of the fine particles, and therefore, some of them fail to take a spherical shape before solidification. It should be noted, however, that the use of ejection nozzles with diameters of the order of hundreds of µm has allowed the preparation of powder with diameters of the order of tens of µm at a low atomization pressure of only 20 bar. Additionally, in the experiments performed in this work, no measures were taken to reduce the appearance of satellites or to avoid particle deformation.

Figure 3 shows the Rietveld refined XRD diffractograms of Fe-N powders with different median diameters, obtained by atomization using the melting nozzle with diameters of 100 µm, 150 µm, 200 µm, and an exposure pressure of 0.5 bar.

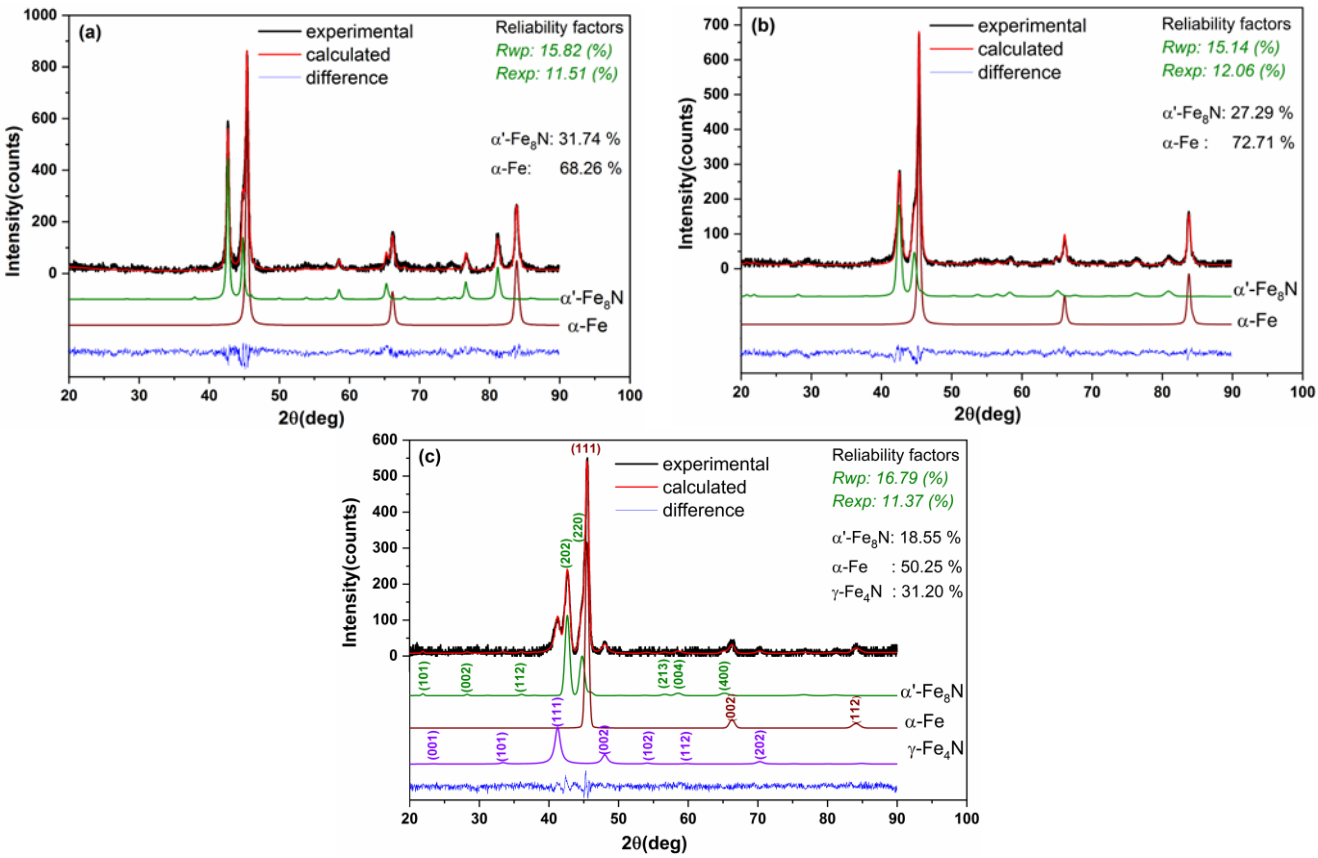

Figure 3. The Rietveld refinement results of Fe-N powders with different median diameters of 32 ± 3 µm (**a**), 58 ± 2 µm (**b**), and 96 ± 2 µm (**c**). The experimentally observed profile (black color), calculated profile (red color), the difference between the calculated and experimental data (blue color), and contribution of specific phases are shown.

The values of goodness factor, $\chi^2 = (R_{wp}/R_{exp})^2$, obtained from the Rietveld refinement for all samples are between 1 and 2, which indicates the quality of the fit. Indeed, in Figure 3, a good agreement can be observed between the experimentally observed and the calculated patterns. The results of XRD patterns analysis indicate that the structure of the powders with diameters of 32 ± 3 µm and 58 ± 2 µm consists of a mixture of α-Fe and α'-Fe_8N crystalline phases, while for the larger powders with a diameter of 96 ± 2 µm, the γ-F_4N phase also appears. For the phase analyses, the cards of indices PDF 98-065-4562 (α'-Fe_8N), PDF 98-015-9354 (iron), and PDF 98-007-9980 (γ-F_4N) were used. The α'-Fe_8N phase percentage decreases from 31.74% corresponding to the powder with diameters of 32 ± 3 µm to 27.29% for those with diameters of 58 ± 2 µm, and 18.55% for 96 ± 2 µm, respectively, suggesting that the percentage of phases depends on the size of the

powders. In fact, it most likely depends on the different speeds of cooling of the powders, an argument in this sense being the appearance of the γ-F_4N phase in large-sized powders due to insufficiently rapid quenching.

The formation mechanism of the α''-$Fe_{16}N_2$ phase consists of the transformation of γ-FeN (austenite) by its quenching to α'-Fe_8N (martensite) and subsequent tempering to α''-$Fe_{16}N_2$ [33,34]. Since the α'-Fe_8N phase is the precursor of the desired α''-$Fe_{16}N_2$ phase, it is therefore desirable that the powders contain a large amount of the α'-Fe_8N phase. But the percentage of the α'-Fe_8N phase is directly proportional to the percentage of the γ-FeN phase, which in turn is dependent on the amount of nitrogen dissolved in the liquid iron. The solubility of nitrogen in iron has been successfully described by Sievert's law, according to which the amount of nitrogen dissolved in the melt is directly proportional to the square root of the gas pressure above the melt, in fact, the exposure pressure [35]. Therefore, to increase the content of the α'-Fe_8N phase in the powders obtained via atomization, we either increase the nitrogen exposure pressure during the induction melting process or decrease the ejection nozzle diameter to prepare powders with even smaller sizes. Due to technological limitations related to the fact that the melting temperature of iron is close to the softening temperature of the quartz tube in which it is heated, reducing the ejection nozzle diameter further was not possible because the nozzle would clog and the quartz tube would break under pressure; therefore, we chose to increase the exposure pressure from 0.5 to 3 bar, keeping the ejection nozzle diameter at 100 µm.

The results from the analysis of X-ray diffraction patterns (not shown here) corresponding to Fe-N powders atomized at nitrogen pressure of 3 bar during the induction melting process showed that the α'-Fe_8N phase fraction increased to 43.32% from 31.74%, which was for the powders prepared at a pressure of 0.5 bar. Therefore, an additional increase in nitrogen pressure during induction melting could lead to an additional increase in the α'-Fe_8N phase content in the atomized powders. However, the atomization plant used by us is a homemade one and does not allow an increase higher than 3 bar, but the challenge remains open for other researchers. Next, only the powders with median diameters of 32 ± 3 µm obtained at 3 bar exposure pressure were nitrided, for which the α'-Fe_8N phase percentage is 43.32%.

Figure 4 shows the phase evolution by XRD patterns of the nitrided powders for 24, 48, and 96 h at a temperature of 150 °C.

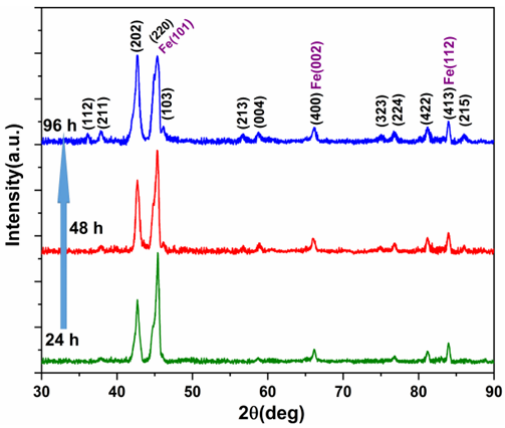

Figure 4. XRD patterns of Fe-N powders nitrided at a temperature of 150 °C for 24, 48, and 96 h.

The α''-$Fe_{16}N_2$ has a structure very similar to α'-Fe_8N except for the arrangement of nitrogen atoms. In the α'-Fe_8N phase, the N atoms are disordered, while in the α''-$Fe_{16}N_2$ phase, they are ordered. For this reason, the most main reflections from the α''-$Fe_{16}N_2$ phase overlap with those from the α'-Fe_8N phase. As can be seen in Figure 4, the nitrided powders showed a diffraction peak at $\theta = 46.57°$ corresponding to the (103) planes, which comes from the ordering of nitrogen atoms and represents the so-called "fingerprint" of the α'' phase [36]. Therefore, this is direct evidence of the occurrence of the α''-$Fe_{16}N_2$ tetragonal

phase (space group: *I*4/*mmm*) (PDF card no. 01-075-2143) in the powders prepared via the gas atomization method followed by their subsequent nitriding in gaseous ammonia. The calculated lattice parameters of the α''-$Fe_{16}N_2$ phase were a = 5.73Å and c = 6.29Å, which are in good agreement with the reported data provided by Kim and Takahashi [34]. Also, it should be mentioned that the (220), (400), and (413) peaks of α''-$Fe_{16}N_2$ shared the intensity with α-Fe(110), α-Fe(200), and α-Fe(112), respectively. It can be observed that the intensity of the (103) peak increased with nitriding time, together with a reduction in α-Fe peaks. In addition, for samples nitrided for 48 or 96 h, the appearance of other new diffraction peaks associated with the α''-$Fe_{16}N_2$ phase is observed. Thus, the volume ratio of the α''-$Fe_{16}N_2$ phase increases with the nitriding time from 38% for powders nitrided for 24 h, reaching 57% after 96 h.

Figure 5a–c show the hysteresis loops of the powders after 24, 48, and 96 h of nitridation time at a temperature of 150 °C. To compare the magnetic properties of nitrided powders with those of powders similar in size from pure Fe, Fe powders atomized in argon gas were prepared, and the corresponding hysteresis loop is shown in Figure 5d.

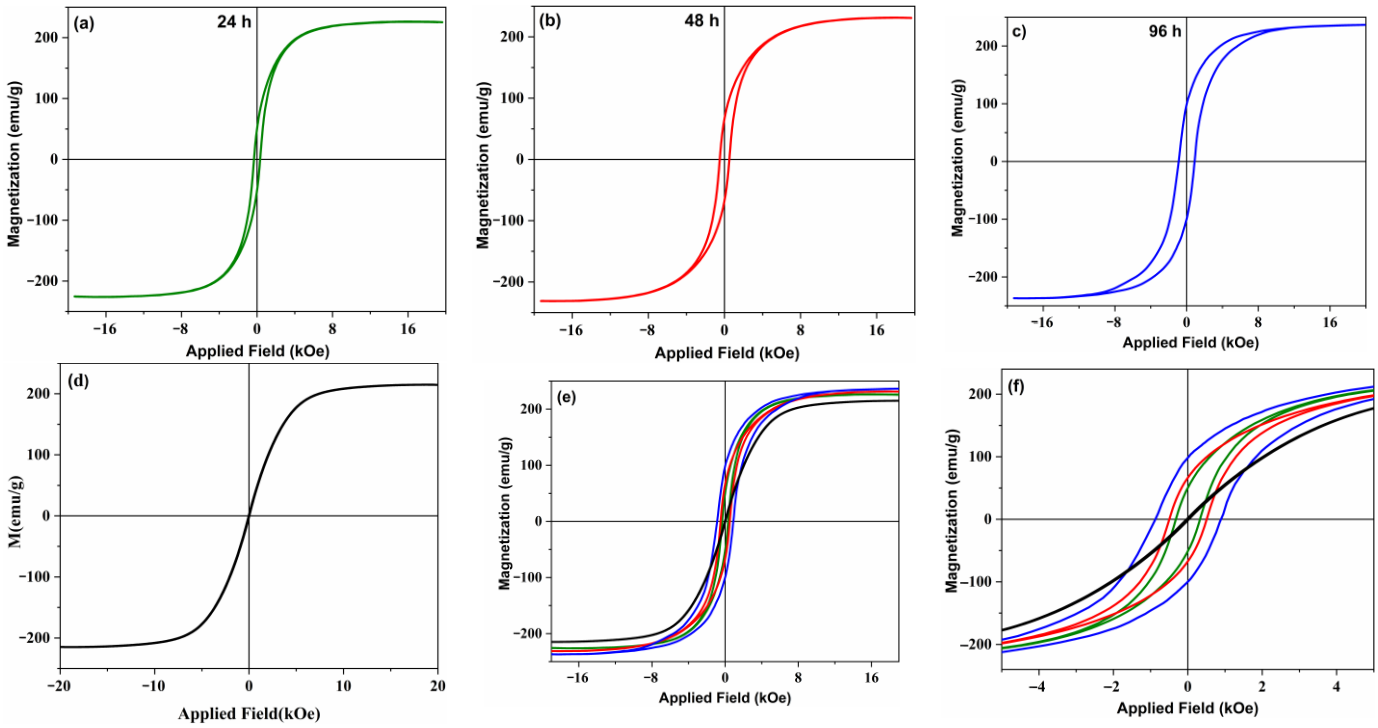

Figure 5. Hysteresis loops: the powders nitrided for (**a**) 24 h, (**b**) 48 h, and (**c**) 96 h; (**d**) iron powders; a comparison between all samples at (**e**) full scale; (**f**) small scale.

The Fe powders atomized in argon showed a saturation magnetization of 215 emu/g and a coercivity about 28 Oe. The saturation magnetization obtained in these powders is lower than the theoretical value of 218 emu/g, most likely due to surface defects or possibly superficial oxidation. For nitrided powders, both the coercivity and the saturation magnetization of the powders increase once the nitriding time increases. Thus, the coercivity increases from approximately 358 Oe for the 24 h nitrided powders to 884 Oe for the 96 h nitrided powders, and the saturation magnetization increases from 224 emu/g to 237 emu/g. Compared to the saturation magnetization of Fe powders atomized in argon, the 96 h nitrided powders show an increase in the saturation magnetization by approximately 10%. The higher values of the coercivity and the saturation magnetization for the sample nitride 96 h are caused by the increase in the percentage of α''-$Fe_{16}N_2$ phase, according to XRD results. However, under the preparation conditions applied in this study, the volume fraction of α''-$Fe_{16}N_2$ is still low. Therefore, although the method described

here opens a new way of preparation of α''-$Fe_{16}N_2$ powders, further future research is needed to optimize the process parameters and increase the volume fraction of α''-$Fe_{16}N_2$.

4. Conclusions

The α''-$Fe_{16}N_2$ powders were successfully obtained via the gas atomization method of pure iron in nitrogen gas, followed by subsequent nitriding in an ammonia–hydrogen gas mixture stream. The atomized powders presented a structure consisting of a mixture of α'-Fe_8N, γ-F_4N, and α-Fe phases. By tuning the parameters of the atomization process, the volume fraction of the α'-Fe_8N phase, which represents the precursor of the desired phase α''-$Fe_{16}N_2$, was increased up to 43.32%. Subsequent nitriding of the powders allowed the transformation of the α'-Fe_8N phase into the α''-$Fe_{16}N_2$ phase. The volume fraction of the α''-$Fe_{16}N_2$ phase in the nitride powders reached a maximum of 57% for which the powders showed a saturation magnetization (Ms) of 237 emu/g, remanence (Mr) of 101 emu/g, and develop reasonable magnetic hardness with coercivity (Hc) of 884 Oe. Taking into account that the ratio of the α''-$Fe_{16}N_2$ phase could be controlled by modifying the nitridation parameters, their further optimization could increase the volume of the α''-$Fe_{16}N_2$ phase and improve the magnetic properties of powders. However, the present results open a new route for the mass-producing of α''-$Fe_{16}N_2$ powder as precursors of permanent magnets without rare earths.

Author Contributions: Conceptualization, funding acquisition, resources, investigation, result discussion, writing original draft, M.G.; sample preparation, experimental design, data analysis, writing original draft, M.L.; investigation, data analysis, results discussion, M.P.; data curation, formal analysis, investigation, equipment assistance, G.S.; experimental design, data analysis, equipment assistance, G.A.; supervision, methodology, results discussion, N.L. All authors have read and agreed to the published version of the manuscript.

Funding: This work was supported by a grant from the Ministry of Research, Innovation and Digitization, CNCS—UEFISCDI, project number PN-III-P4-PCE-2021-0298, within PNCDI III.

Data Availability Statement: Data supporting the reported results are available from the corresponding author upon request.

Conflicts of Interest: The authors declare no conflict of interest.

References

1. McCallum, R.; Lewis, L.; Skomski, R.; Kramer, M.; Anderson, I. Practical Aspects of Modern and Future Permanent Magnets. *Annu. Rev. Mater. Res.* **2014**, *44*, 451–477. [CrossRef]
2. Coey, J.M.D. Perspective and Prospects for Rare Earth Permanent Magnets. *Engineering* **2020**, *6*, 119–131. [CrossRef]
3. Giannopoulos, G.; Barucca, G.; Kaidatzis, A.; Psycharis, V.; Salikhov, R.; Farle, M.; Koutsoufakis, E.; Niarchos, D.; Mehta, A.; Scuderi, M.; et al. L10-FeNi flms on Au-Cu-Ni bufer-layer: A high-throughput combinatorial study. *Sci. Rep.* **2018**, *8*, 15919. [CrossRef] [PubMed]
4. Kim, J.; Kim, S.; Suh, J.-Y.; Kim, Y.J.; Kim, Y.K.; Choi-Yim, H. Properties of a rare earth free L10-FeNi hard magnet developed through annealing of FeNiPC amorphous ribbons. *Curr. Appl. Phys.* **2019**, *19*, 599–605. [CrossRef]
5. Jensen, B.A.; Tang, W.; Liu, X.; Nolte, A.I.; Ouyang, G.; Dennis, K.W.; Cui, J. Optimizing composition in MnBi permanent magnet alloys. *Acta Mater.* **2019**, *181*, 595–602. [CrossRef]
6. Cui, J.; Choi, J.P.; Li, G.; Polikarpov, E.; Darsell, J.; Overman, N.; Olszta, M.; Schreiber, D.; Bowden, M.; Droubay, T.; et al. Thermal stability of MnBi magnetic materials. *J. Phys. Condens. Matter* **2014**, *26*, 064212. [CrossRef]
7. Roman, T.; Murgulescu, I.-I.; Ababei, G.; Stoian, G.; Lostun, M.; Porcescu, M.; Grigoras, M.; Lupu, N. Facile method of raising the LTP content in Mn-Bi alloys by using sequential separation techniques for Bi and Mn. *Mater. Today Commun.* **2022**, *33*, 104241. [CrossRef]
8. Odkhuu, D.; Hong, S.C. Simultaneous tuning of the magnetic anisotropy and thermal stability of α''-phase $Fe_{16}N_2$. *Sci. Rep.* **2021**, *11*, 7823. [CrossRef]
9. Ochirkhuyag, T.; Hong, S.C.; Odkhuu, D. First-Principles Prediction of Enhanced Magnetic Anisotropy of α''-Phase $Fe_{16}N_2$ with B and C Impurities. *IEEE Trans. Magn.* **2021**, *57*, 7000103. [CrossRef]
10. Ji, N.; Allard, L.F.; Lara-Curzio, E.; Wang, J.-P. N site ordering effect on partially ordered $Fe_{16}N_2$. *Appl. Phys. Lett.* **2011**, *98*, 092506. [CrossRef]

11. Li, X.; Yang, M.; Jamali, M.; Shi, F.; Kang, S.; Jiang, Y.; Zhang, X.; Li, H.; Okatov, S.; Faleev, S.; et al. Heavy-Metal-Free, Low-Damping, and Non-Interface Perpendicular $Fe_{16}N_2$ Thin Film and Magnetoresistance Device. *Phys. Status Solidi Rapid Res. Lett.* **2019**, *13*, 1900089. [CrossRef]
12. Hang, X.; Zhang, X.; Ma, B.; Lauter, V.; Wang, J.-P. Epitaxial $Fe_{16}N_2$ thin film on nonmagnetic seed layer. *Appl. Phys. Lett.* **2018**, *112*, 192402. [CrossRef]
13. Zhang, X.; Nomura, K.; Wang, J.-P. New insight on the Mössbauer spectra for $Fe_{16}N_2$ thin films with high saturation magnetization. *Jpn. J. Appl. Phys.* **2019**, *58*, 120907. [CrossRef]
14. Jiang, Y.; Mehedi, M.A.; Fu, E.; Wang, Y.; Allard, L.F.; Wang, J.-P. Synthesis of $Fe_{16}N_2$ compound Free-Standing Foils with 20 MGOe Magnetic Energy Product by Nitrogen Ion-Implantation. *Sci. Rep.* **2016**, *6*, 25436. [CrossRef] [PubMed]
15. Liu, J.; Guo, G.; Zhang, X.; Zhang, F.; Ma, B.; Wang, J.-P. Synthesis of α''-$Fe_{16}N_2$ foils with an ultralow temperature coefficient of coercivity for rare-earth-free magnets. *Acta Mater.* **2020**, *184*, 143–150. [CrossRef]
16. Jiang, Y.; Dabade, V.; Allard, L.F.; Lara-Curzio, E.; James, R.; Wang, J.-P. Synthesis of $\alpha''-Fe_{16}N_2$ Compound Anisotropic Magnet by the Strained-Wire Method. *Phys. Rev. Appl.* **2016**, *6*, 024013. [CrossRef]
17. Liu, J.; Guo, G.; Zhang, F.; Wu, Y.; Ma, B.; Wang, J.-P. Synthesis of α''-$Fe_{16}N_2$ ribbons with a porous structure. *Nanoscale Adv.* **2019**, *1*, 1337–1342. [CrossRef] [PubMed]
18. Li, Y.; Kuang, Q.; Men, X.; Wang, S.; Li, D.; Choi, C.; Zhang, Z. Anisotropic Growth and Magnetic Properties of α''-$Fe_{16}N_2$@C Nanocones. *Nanomaterials* **2021**, *11*, 890. [CrossRef]
19. Dirba, I.; Schwöbel, C.A.; Diop, L.V.B.; Duerrschnabel, M.; Molina-Luna, L.; Hofmann, K.; Komissinskiy, P.; Kleebe, H.-J.; Gutfleisch, O. Synthesis, morphology, thermal stability and magnetic properties of α''-$Fe_{16}N_2$ nanoparticles obtained by hydrogen reduction of γ-Fe_2O_3 and subsequent nitrogenation. *Acta Mater.* **2017**, *123*, 214–222. [CrossRef]
20. Li, J.; Yuan, W.; Peng, X.; Yang, Y.; Xu, J.; Wang, X.; Hong, B.; Jin, H.; Jin, D.; Ge, H. Synthesis of fine a α''-$Fe_{16}N_2$ powders by low-temperature nitridation of α-Fe from magnetite nanoparticles. *AIP Adv.* **2016**, *6*, 125104. [CrossRef]
21. Ji, N.; Lauter, V.; Zhang, X.; Ambaye, H.; Wang, J.-P. Strain induced giant magnetism in epitaxial $Fe_{16}N_2$ thin film. *Appl. Phys. Lett.* **2013**, *102*, 072411. [CrossRef]
22. Jiang, Y.; Liu, J.; Suri, P.K.; Kennedy, G.; Thadhani, N.N.; Flannigan, D.J.; Wang, J.-P. Preparation of an α''-$Fe_{16}N_2$ Magnet via a Ball Milling and Shock Compaction Approach. *Adv. Eng. Mater.* **2016**, *18*, 1009–1016. [CrossRef]
23. Kim, J.; Hwang, J.; Yi, S. Iron nitride based magnetic powder synthesized by mechanical alloying of Fe-based glassy powders and solid nitrogen compounds. *J. Magn. Magn. Mater.* **2021**, *539*, 168329. [CrossRef]
24. Tobise, M.; Saito, S. Synthesis of α''-$(Fe,M)_{16}N_2$ Nanoparticles Obtained by Hydrogen Reduction and Subsequent Nitridation Starting From α-(Fe,M)OOH (M = Co, Al). *IEEE Trans. Magn.* **2022**, *58*, 1–5. [CrossRef]
25. Ogi, T.; Li, Q.; Horie, S.; Tameka, A.; Iwaki, T.; Okuyama, K. High-purity core-shell α''-$Fe_{16}N_2/Al_2O_3$ nanoparticles synthesized from α-hematite for rare-earth-free magnet applications. *Adv. Powder Technol.* **2016**, *27*, 2520–2525. [CrossRef]
26. Zulhijah, R.; Nandiyanto, A.B.D.; Ogi, T.; Iwaki, T.; Nakamura, K.; Okuyama, K. Effect of oxidation on α''-$Fe_{16}N_2$ phase formation from plasma-synthesized spherical core–shell α-Fe/Al_2O_3 nanoparticles. *J. Magn. Magn. Mater.* **2015**, *381*, 89–98. [CrossRef]
27. Zulhijah, R.; Nandiyanto, A.B.D.; Ogi, T.; Iwaki, T.; Nakamura, K.; Okuyama, K. Gas phase preparation of spherical core–shell α''-$Fe_{16}N_2/SiO_2$ magnetic nanoparticles. *Nanoscale* **2014**, *6*, 6467–6491. [CrossRef] [PubMed]
28. Antipas, G.S.E. Review of gas atomisation and spray forming phenomenology. *Powder Met.* **2013**, *56*, 317–330. [CrossRef]
29. Kassym, K.; Perveen, A. Atomization processes of metal powders for 3D printing. *Mater. Today Proc.* **2020**, *26*, 1727–1733. [CrossRef]
30. Sun, P.; Fang, Z.Z.; Zhang, Y.; Xia, Y. Review of the Methods for Production of Spherical Ti and Ti Alloy Powder. *JOM* **2017**, *69*, 1853–1860. [CrossRef]
31. Sarriegui, G.; Martín, J.; Burgos, N.; Ipatov, M.; Zhukov, A.; Gonzalez, J. Effect of particle size on grain growth of Nd-Fe-B powders produced by gas atomization. *Mater. Charact.* **2022**, *187*, 111824. [CrossRef]
32. Grigoras, M.; Lostun, M.; Stoian, G.; Ababei, G.; Porcescu, M.; Lupu, N. The Influence of Preparation Parameters on the Morphology and Magnetic Properties of Fe-N Powders Obtained by the Gas Atomization Method. *Appl. Sci.* **2023**, *13*, 11529. [CrossRef]
33. Jack, K.H. The occurrence and the crystal structure of α''-iron nitride; a new type of interstitial alloy formed during the tempering of nitrogen-martensite. *Proc. R. Soc. Lond. Ser. A Math. Phys. Sci.* **1951**, *208*, 216–224. [CrossRef]
34. Jack, K. The synthesis and characterization of bulk α''-$Fe_{16}N_2$. *J. Alloys Compd.* **1995**, *222*, 160–166. [CrossRef]
35. Sieverts, A.; Zapf, G. Eisen und Stickstoff. *Z. Phys. Chem.* **1935**, *172*, 314–315. [CrossRef]
36. Kojima, T.; Kameoka, S.; Mizuguchi, M.; Takanashi, K.; Tsai, A.-P. FeNi and $Fe_{16}N_2$ Magnets Prepared Using Leaching. *Mater. Trans.* **2019**, *60*, 1066–1071. [CrossRef]